New Phytologist

New Phytologist Supporting Information

Article title: Plant profit maximisation improves predictions of European forest responses to drought

Authors: Manon E. B. Sabot, Martin G. De Kauwe, Andy J. Pitman, Belinda E. Medlyn, Anne Verhoef, Anna M. Ukkola, and Gab Abramowitz.

Article acceptance date: 03 December 2019

The following Supporting Information is available for this article:

Fig. S1 A schematic showing the modelling experiments.

Fig. S2 A 14-day running average of the carbon and water fluxes predicted by the Control model at the five northernmost eddy-covariance sites during the 2003 and 2006 European drought events, compared with the CABLE LSM and with the observations.

Fig. S3 A 14-day running average of the carbon and water fluxes predicted by the Control model at the five southernmost eddy-covariance sites during the 2003 and 2006 European drought events, compared with the CABLE LSM and with the observations.

Fig. S4 The predawn volumetric soil water available to the vegetation, as simulated by the Control model and by CABLE, at the five northernmost eddy-covariance sites during the 2003 European drought event.

Fig. S5 The predawn volumetric soil water available to the vegetation, as simulated by the Control model and by CABLE, at the five southernmost eddy-covariance sites during the 2003 European drought event.

Fig. S6 A 14-day running average of the carbon and water fluxes predicted by two different calibrations of the Control model at a sub-selection of sites in 2002, 2003, 2005, and 2006, compared with the calibrated $Profit_{max}$ model, with the reference Control model, and with the observations.

Fig. S7 A 14-day running average of the carbon and water fluxes predicted by the best selected Calibration at the five northernmost eddy-covariance sites in 2002 and 2005, compared with the Control model and with the observations.

Fig. S8 A 14-day running average of the carbon and water fluxes predicted by the best selected Calibration at the five southernmost eddy-covariance sites in 2002 and 2005, compared with the Control model and with the observations.

Fig. S9 The stomatal conductance as a function of the predawn total volumetric soil water available to the vegetation.

Table S1 Soil parameters at the 10 eddy-covariance sites

Table S2 Plant trait inputs at the 10 eddy-covariance sites

Table S3 Surface properties per plant functional type (PFT)

Table S4 Water available in the five soil-sub layers located below the soil top layer

Table S5 Parameters used in the biochemical photosynthesis model

Table S6 Predicted ranges of k_{max} at the 10 sites compared with species-specific measured values of k_{max}

Methods S1 Biochemical photosynthesis model

Methods S2 Energy balance model

Methods S3 Shape of the vulnerability curves

Methods S4 Coupling carbon and water

Methods S5 Scaling from leaf to canopy

Methods S6 Soil hydrology

Methods S7 Prescribed LAI

Methods S8 Parameter calibrations

Notes S1 Comparison of the Control with CABLE

Notes S2 Why did we not calibrate the Control model?

Notes S3 Comparison of the predicted values of k_{max} to the literature

Supporting Information Figures

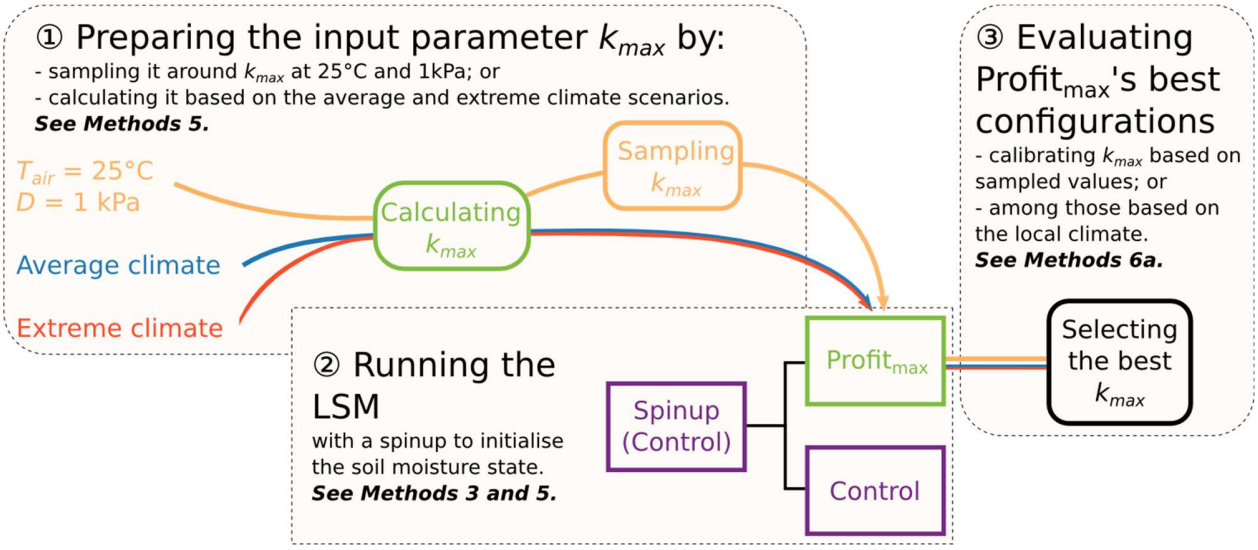

Fig. S1 A schematic showing the modelling experiments, from **(1)** estimating the maximum hydraulic conductance (k_{max}) parameter, to **(2)** running the experiments, and **(3)** evaluating the best model configurations.

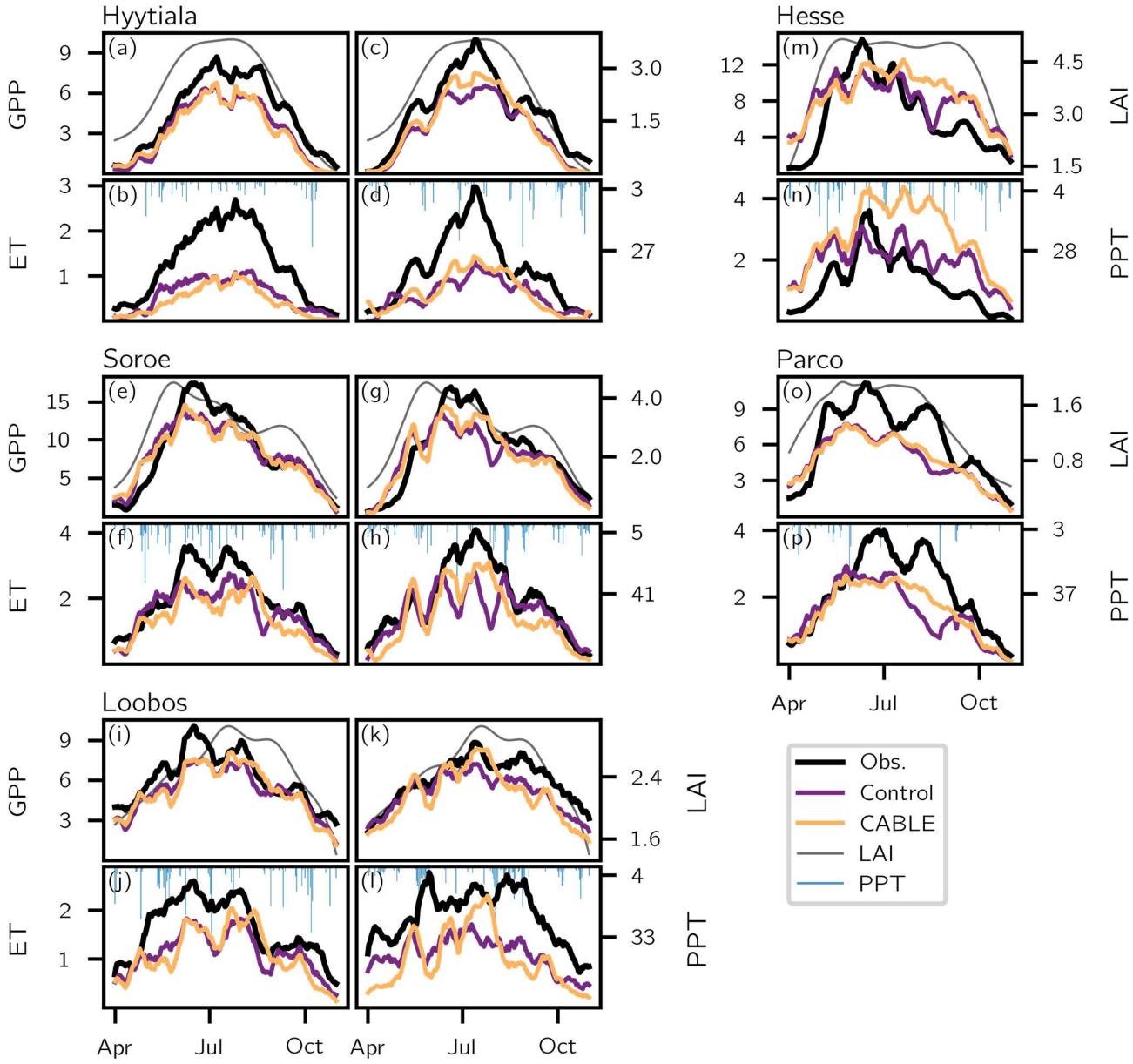

Fig. S2 A 14-day running average of the carbon and water fluxes predicted by the Control model (purple line) at the five northernmost eddy-covariance sites during the 2003 (panels a, b, e, f, i, j, m, n, o, p) and 2006 (panels c, d, g, h, k, l) European drought events, compared with the CABLE LSM (orange line), and with the observations (black line). Grey lines show the prescribed phenologies (LAI, m^2 m^{-2}) and blue bars the daily precipitation (PPT, mm d^{-1}). The Gross Primary Productivity (GPP) is in g C m^{-2} d^{-1} and the Evapotranspiration (ET) in mm d^{-1}.

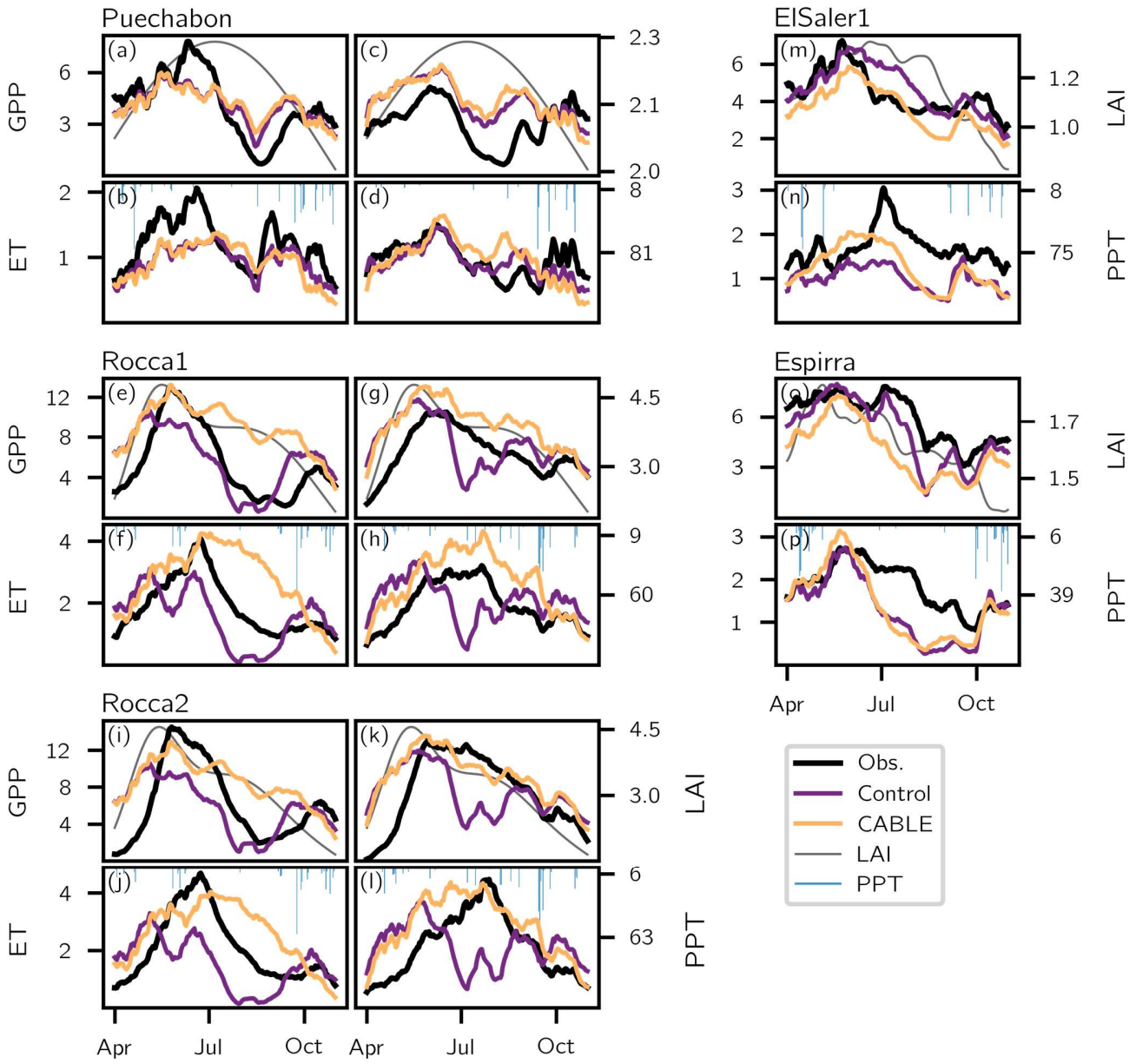

Fig. S3 A 14-day running average of the carbon and water fluxes predicted by the Control model (purple line) at the five southernmost eddy-covariance sites during the 2003 (panels a, b, e, f, i, j, m, n, o, p) and 2006 (panels c, d, g, h, k, l) European drought events, compared with the CABLE LSM (orange line), and with the observations (black line). Grey lines show the prescribed phenologies (LAI, m^2 m^{-2}) and blue bars the daily precipitation (PPT, mm d^{-1}). The Gross Primary Productivity (GPP) is in g C m^{-2} d^{-1} and the Evapotranspiration (ET) in mm d^{-1}.

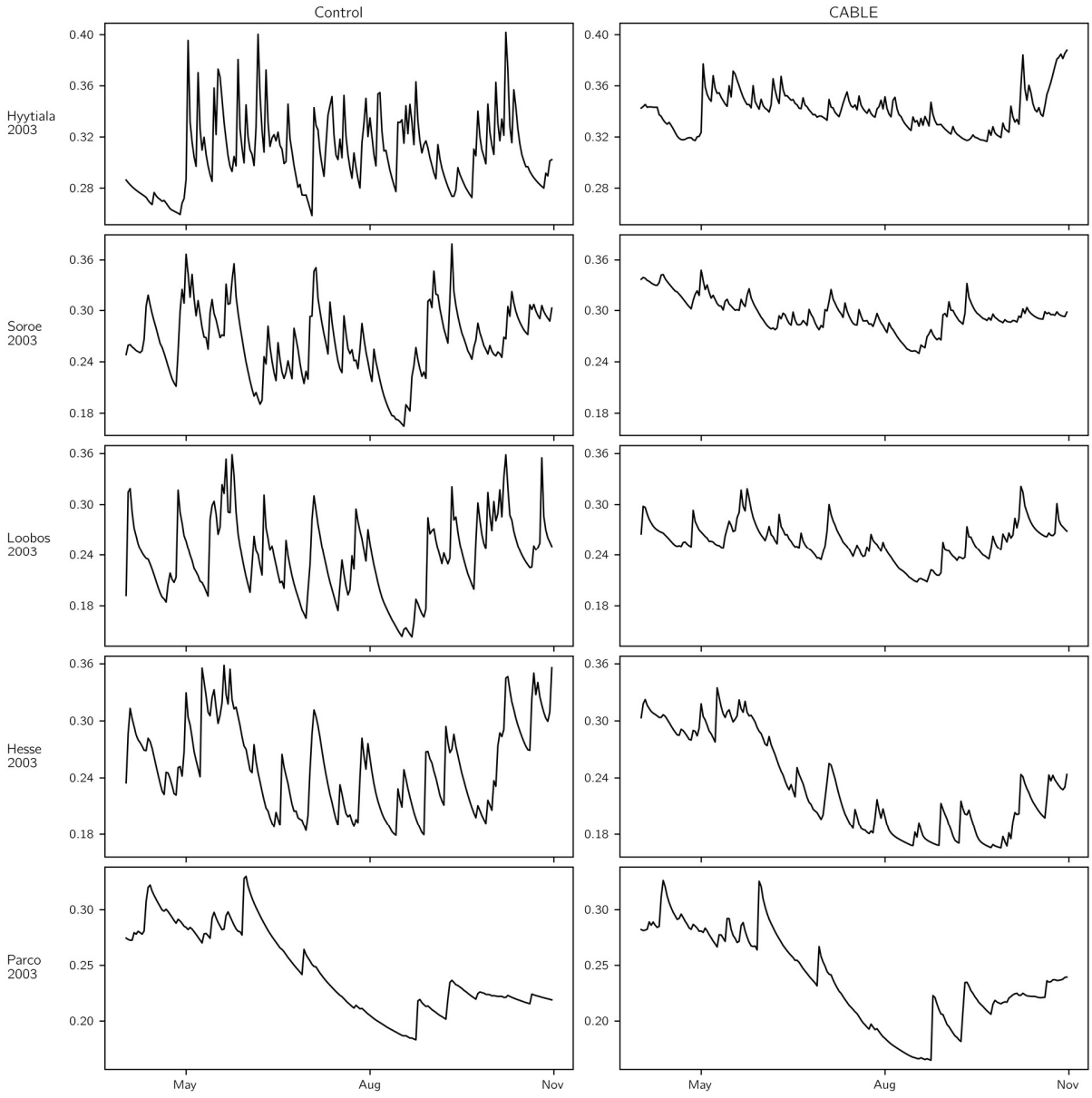

Fig. S4 The predawn volumetric soil water (m^2 m^{-2}) available to the vegetation between April-November, as simulated by the Control model (left column) and by CABLE (right column), at the five northernmost eddy-covariance sites during the 2003 European drought event.

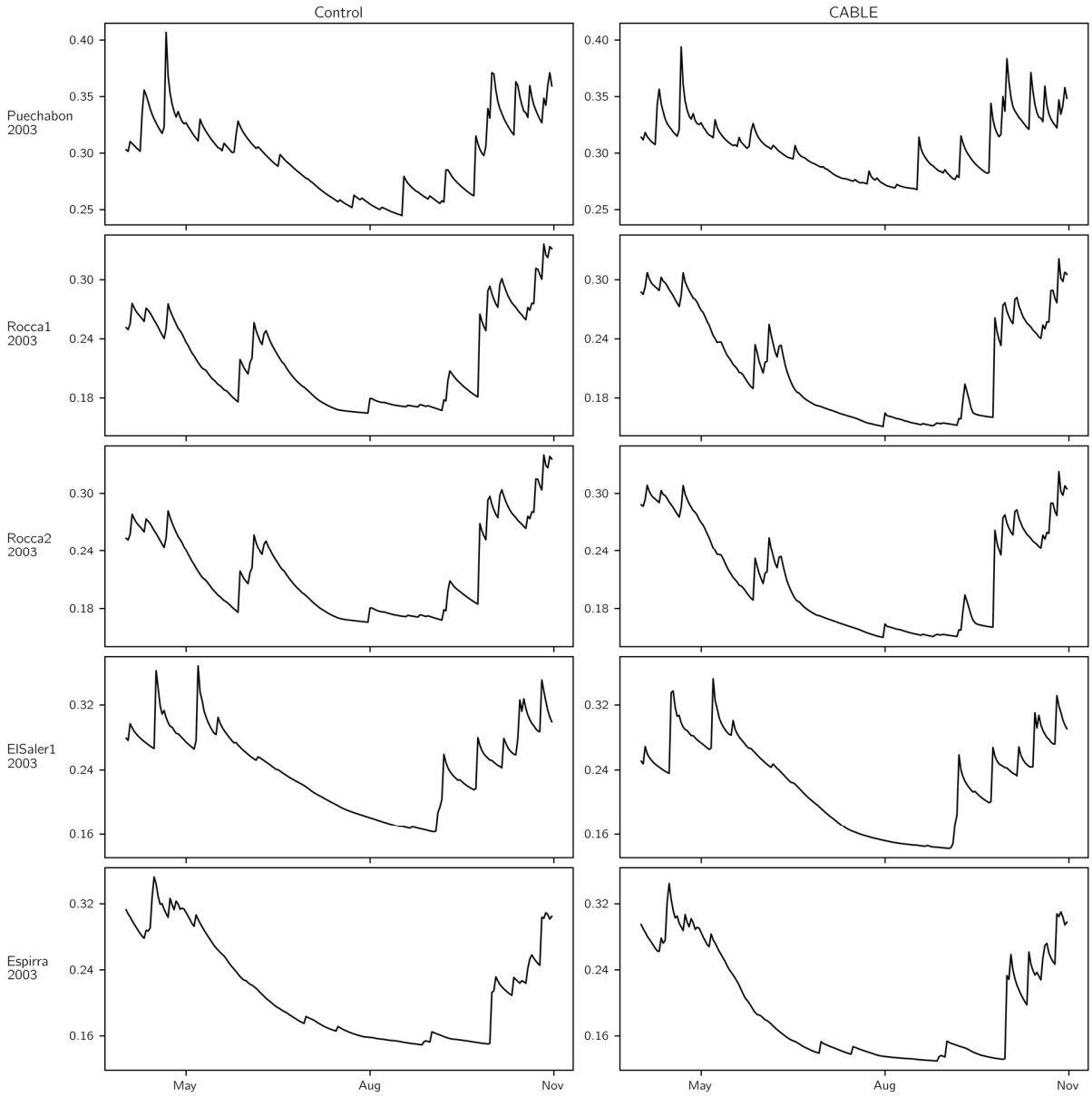

Fig. S5 The predawn volumetric soil water (m^2 m^{-2}) available to the vegetation between April-November, as simulated by the Control model (left column) and by CABLE (right column), at the five southernmost eddy-covariance sites during the 2003 European drought event.

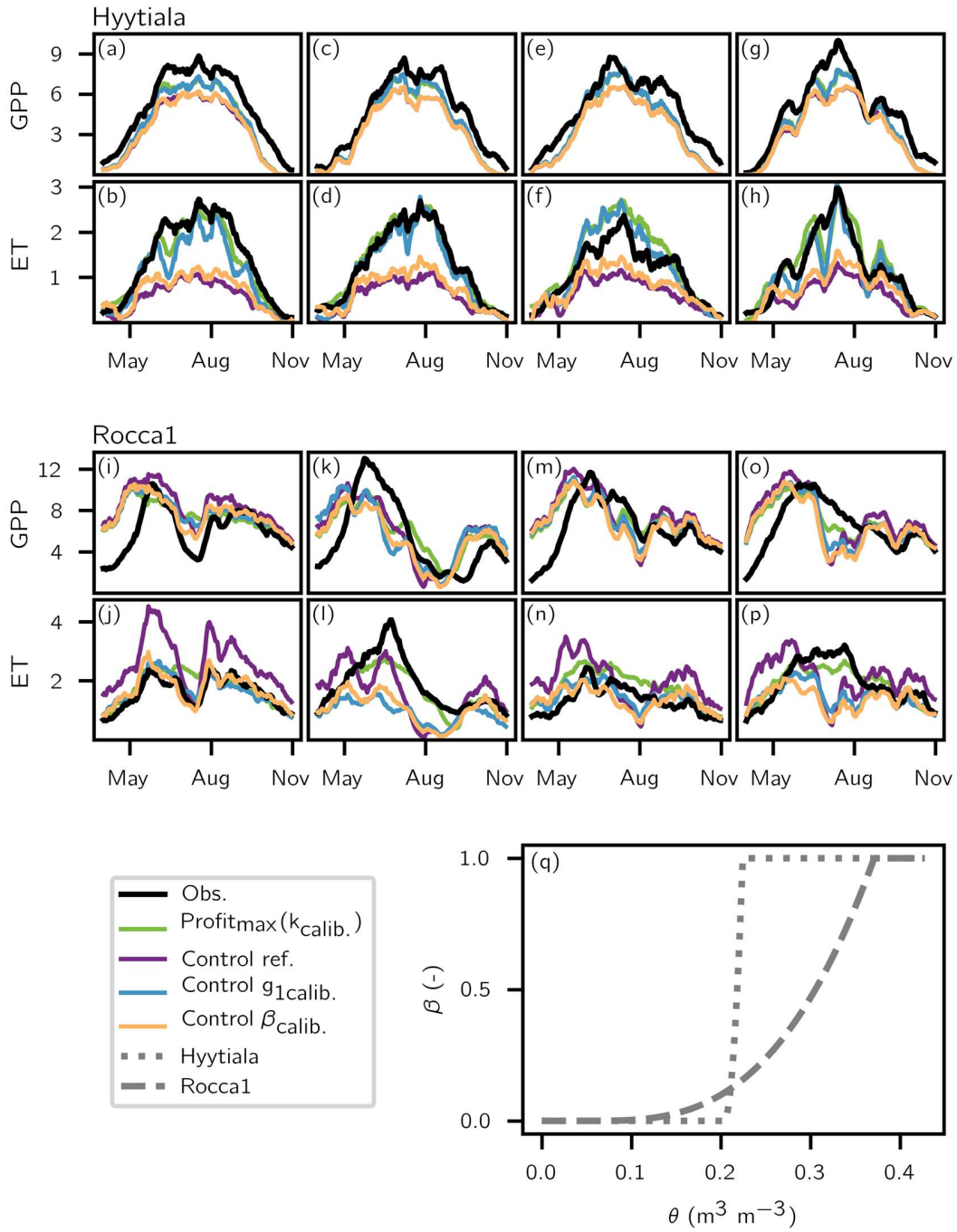

Fig.S6 A 14-day running average of the carbon and water fluxes predicted by two different calibrations of the Control model (blue and orange lines) at a sub-selection of two sites in 2002 (panels a, b, i, j), 2003 (panels c, d, k, l), 2005 (e, f, m, n), and 2006 (g, h, o, p), compared with the calibrated $Profit_{max}$ model (green line), with the reference Control model (purple line), and with the observations (black line). The Gross Primary Productivity (GPP) is in g C m^{-2} d^{-1} and the Evapotranspiration (ET) in mm d^{-1}. Panel **(q)** shows the markedly different calibrated soil moisture stress factors (β, unitless) as a function of volumetric soil moisture (θ) at the two sites.

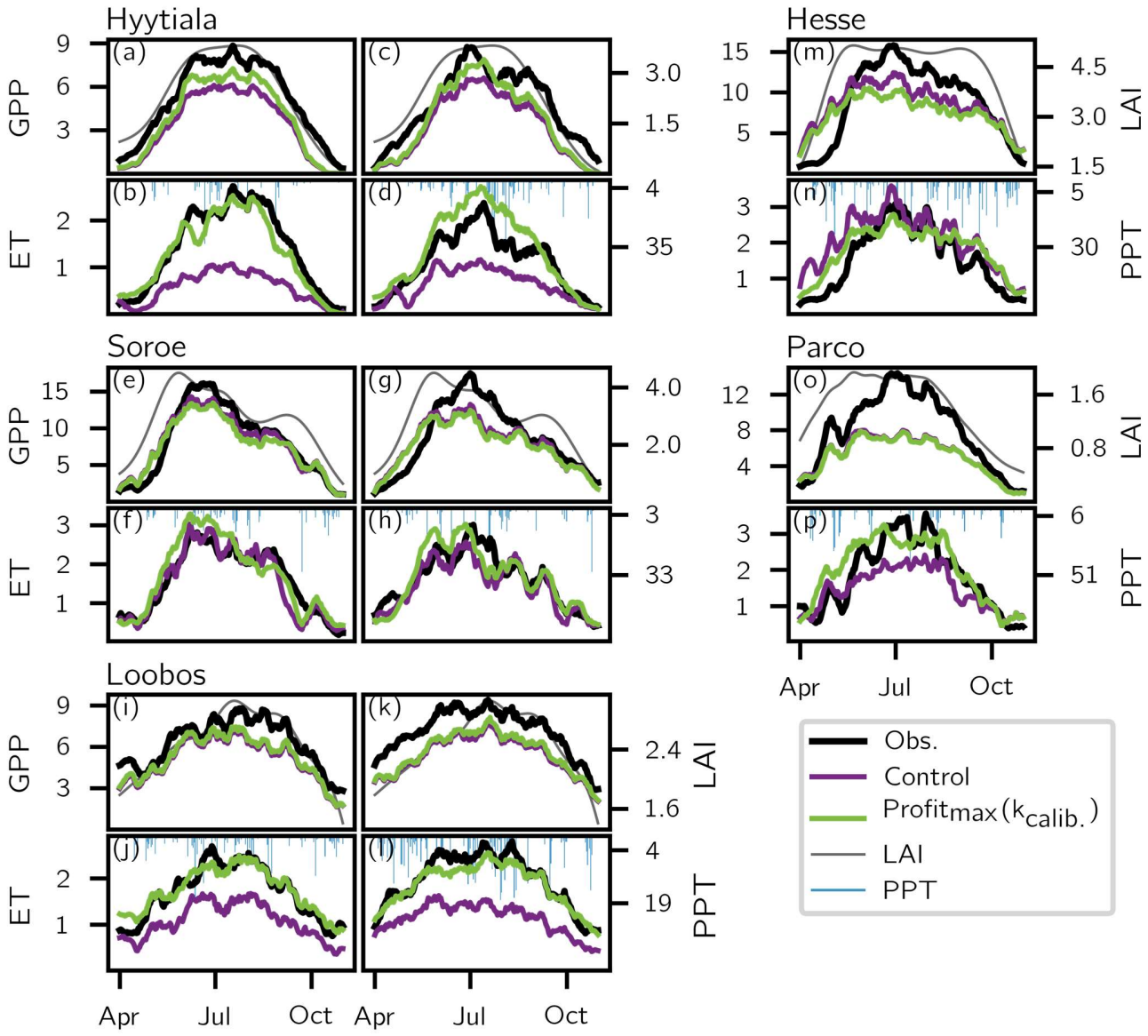

Fig. S7 A 14-day running average of the carbon and water fluxes predicted by the best selected Calibration (green line) at the five northernmost eddy-covariance sites in 2002 (panels a, b, e, f, i, j, m, n, o, p) and 2005 (panels c, d, g, h, k, l), compared with the Control model (purple), and with the observations (black line). Grey lines show the prescribed phenologies (LAI, m^2 m^{-2}) and blue bars the daily precipitation (PPT, mm d^{-1}). The Gross Primary Productivity (GPP) is in g C m^{-2} d^{-1} and the Evapotranspiration (ET) in mm d^{-1}.

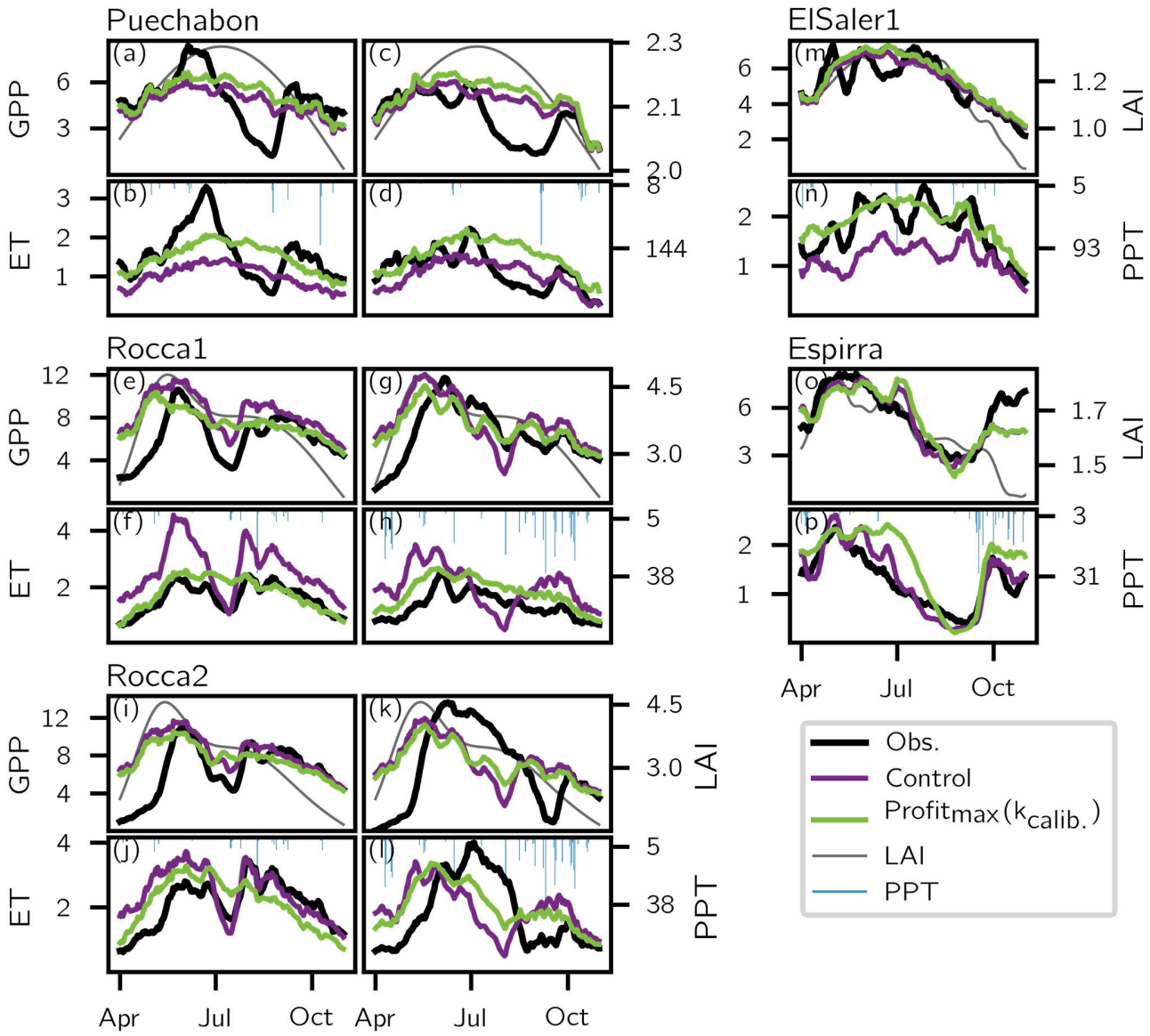

Fig. S8 A 14-day running average of the carbon and water fluxes predicted by the best selected Calibration (green line) at the five southernmost eddy-covariance sites in 2002 (panels a, b, e, f, i, j, m, n, o, p) and 2005 (panels c, d, g, h, k, l), compared with the Control model (purple), and with the observations (black line). Grey lines show the prescribed phenologies (LAI, m^2 m^{-2}) and blue bars the daily precipitation (PPT, mm d^{-1}). The Gross Primary Productivity (GPP) is in g C m^{-2} d^{-1} and the Evapotranspiration (ET) in mm d^{-1}.

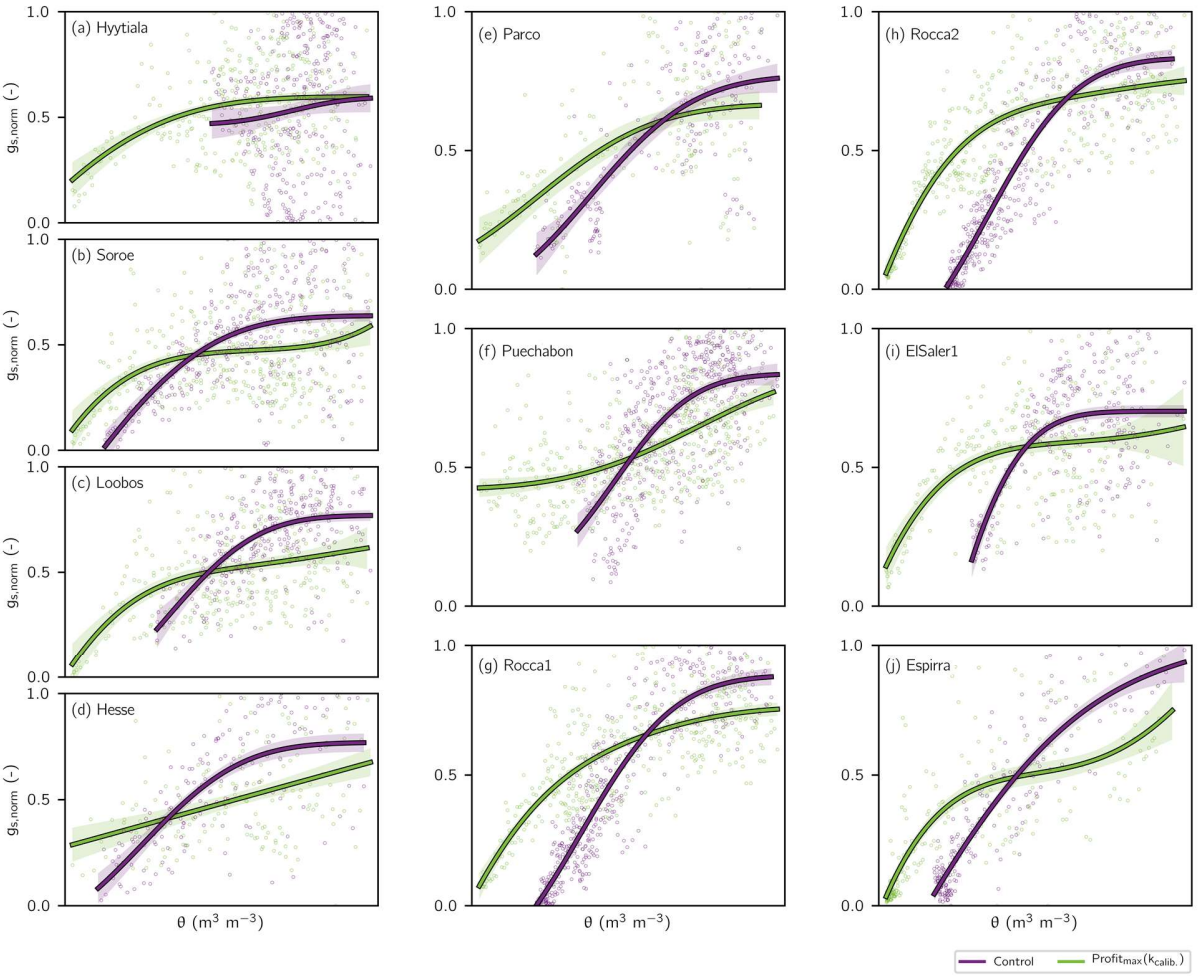

Fig. S9 The stomatal conductance (g_s), as a function of the predawn total volumetric soil water available to the vegetation (θ). The functional forms of the g_s - θ curves, for the best Calibration (green) and the Control model (purple), are made comparable by normalising g_s. To avoid low solar radiation and low temperature effects, the g_s data were restricted between 9:00 h – 15:00 h from April – November across all years. Individual dots represent all the remaining data points; the curves were fitted using a linear generalised additive model and the shadings show the 95% confidence interval of the fit.

Supporting Information Tables

Table S1 Soil parameters at the 10 eddy-covariance sites

Site name	Ψ_{aep}[a] (-kPa)	k_{sat}[b] (µm s^{-1})	θ_{sat}[c] (m^3 m^{-3})	θ_{fc}[d] (m^3 m^{-3})	θ_{wp}[e] (m^3 m^{-3})	b_{CH}[f] (-)	r_{soil}[g] (%)	Z_{total}[h] (m)
Hyytiälä	1.78	5.17	0.428	0.274	0.153	6.57	0.2	0.28
Sorø	1.62	5.71	0.424	0.265	0.146	6.43	0.2	0.32
Loobos	1.12	9.31	0.408	0.213	0.103	5.22	0.2	0.25
Hesse Forest-Sarrebourg	1.50	5.62	0.421	0.269	0.154	6.86	0.2	0.41
Parco Ticino Forest	1.48	6.23	0.420	0.257	0.141	6.33	0.2	1.47
Puéchabon	1.51	5.27	0.422	0.275	0.162	7.22	0.4	1.36
Roccarespampani 1&2	1.66	5.39	0.425	0.271	0.153	6.64	0.2	1.07
El Saler 1	1.05	8.83	0.406	0.225	0.117	5.84	0.4	1.25
Espirra	1.24	7.13	0.413	0.246	0.135	6.34	0.4	1.26

All parameters except total effective rooting depth (Z_{total}) and percentage resistance to soil evaporation (r_{soil}) were determined based on the Zobler soil texture types (Zobler, 1999) and CABLE's ancillary files for soil physical properties**.**

[a] Air entry point water potential

[b] Soil hydraulic conductivity at saturation

[c] Volumetric soil water content at saturation

[d] Volumetric soil water content at field capacity

[e] Volumetric water content at wilting point, θ_{wp} is only used in the control model for the regulation of gas-exchanges (in the soil moisture stress function, β, see Eqn 7 of the Main text)

[f] b_{CH} is the Clapp-Hornberger pore size distribution index for soil-water retention functions, relating the average volumetric soil moisture and the soil water potential across layers (Clapp & Hornberger, 1978; Duursma *et al.*, 2008)

[g] Percentage resistance to evaporation from the top soil layer. This parameter is applied to limit soil evaporation biases, not unlike the approach of Van den Hoof *et al.* (2013)

[h] Total effective rooting depth, or bucket depth. The procedure by which these values were obtained is detailed in Methods S8a

Table S2 Plant trait inputs at the 10 eddy-covariance sites

Site name	**$V_{cmax,25}$**[a] ($\mu mol\ s^{-1}\ m^{-2}$)	**$R_{d,25}$**[b] ($\mu mol\ s^{-1}\ m^{-2}$)	**g_1**[c] ($kPa^{0.5}$)	**P_{50}**[d] (-MPa)	**P_{88}**[d] (-MPa)
Hyytiälä	23.36 *	0.35	1.29 ***	3.09	3.45
Sorø	80.10 *	1.20	3.66 ***	3.15	3.67
Loobos	37.07 *	0.56	2.35	3.09	3.45
Hesse Forest-Sarrebourg	80.10 *	1.20	4.45	3.15	3.67
Parco Ticino Forest	57.70	0.87	4.45	1.80 ****	2.70 ****
Puéchabon	40.00 **	0.60	1.56 ***	6.90	9.43
Roccarespampani 1&2	57.70	0.87	4.45	4.56 ****	8.38 ****
El Saler1	62.50	0.94	2.35	5.14	5.61
Espirra	61.40	0.92	4.11	4.12 *****	4.5 *****

[a] Maximum carboxylation rate at 25°C. Values that are not marked with a symbol are PFT-level values from (Kattge *et al.*, 2009). Marked values are reported valid at the site-level. For * see table 8.2 in Valentini (2003) and for ** see table 3.1 in Martin-StPaul (2012)

[b] Dark respiration rate at 25°C. By default, $R_{d,25}$ is set to $0.015\ V_{cmax,25}$

[c] g1 is a parameter input solely used by the Control model (Medlyn *et al.*, 2011). Unmarked values are PFT-based, as presented in De Kauwe *et al.* (2015). For *** see the on-site measurements presented in Lin *et al.* (2015)

[d] P_{50} and P_{88} are the plant hydraulic traits used to derive the plant vulnerability curves. All the P_{50} and P_{88} parameters which we used are species-level averages for the dominant species (cf. Table 1 of the Main text) at the site. Unmarked data originate from the Sureau database (Martin-StPaul *et al.*, 2017). From the parameter values provided in the Sureau database, we retrieved the P_{88}, using a Weibull distribution function, and the P_{12} and P_{50}. For **** the P_{50} and P_{88} parameter values of the dominant species were absent from both the Sureau database and the Choat *et al.* (2012) dataset. We therefore used P_{50} and P_{88} of species within the same genus, naturally reaching comparable maximum heights and occurring in similar climatic ranges. Those species traits were found in the Choat *et al.* (2012) dataset and are, respectively, those of: *Populus balsamifera,* and *Quercus frainetto*. For ***** see Lucani *et al.* (2019)

Table S3 Surface properties per plant functional type (PFT)

Parameter description	DBF[a]	EBF[a]	ENF[a]	All	Unit
maximum leaf width[b]	0.080	0.050	0.001		m
canopy rainfall intercept[c]	0.250	0.250	0.150		%
leaf albedo[b]	0.092	0.076	0.062		-
wet soil albedo[d]				0.100	-
dry soil albedo[e]				0.250	-
leaf emissivity[f]				0.970	-
soil emissivity[f]				0.945	-

[a] PFTs are defined as: evergreen needleleaf forest (ENF), evergreen broadleaf forest (EBF), deciduous broadleaf forest (DBF)

[c] the percentage canopy interception accounts for the amount of rain that does not percolate through the canopy to the soil, alike CABLE's canopy rainfall interception parameter

[b] from CABLE's ancillary files for vegetation properties

[d] from CABLE's ancillary files for vegetation properties and table 11.2 in Campbell & Norman (1998)

[e] from Berge (1990). The dry soil albedo replaces the wet soil albedo when the top soil layer moisture content drops below $0.5 \times (\theta_{fc} - \theta_{wp})$

[f] from table 11.3 in Campbell & Norman (1998)

Table S4 Water available in the five soil-sub layers located below the soil top layer

Soil sub-layer	% of total water availability (excluding top soil layer)
2	28.85
3	42.33
4	26.20
5	2.608
6	0.004

The water available in the five soil sub-layers is relative to total water availability and determined from CABLE's ancillary files for percentage root water access across the five deepest layers.

Table S5 Parameters used in the biochemical photosynthesis model

Abbreviation	Parameter description	Value	Unit
C_a	atmospheric CO_2 concentration	37.00	Pa
O_a	atmospheric O_2 concentration	20.73	kPa
Γ^*_{25}	CO_2 compensation point at 25°C	4.22	Pa
K_c	Michaelis-Menten constant for carboxylation	39.96	Pa
K_o	Michaelis-Menten constant for oxygenation	27.48	kPa
$J_{max,25}$: $V_{cmax,25}$	$J_{max,25}$ to $V_{cmax,25}$ ratio	1.67	-
α	quantum yield of electron transport	0.30	mol photon mol^{-1} electron
c	curvature of the light response	0.7	-
h	transition curvature factor	0.99	-
E_c	energy of activation of the carboxylation	79430	J mol^{-1}
E_o	energy of activation of the oxygenation	36380	J mol^{-1}
E_v	energy of activation of V_{cmax}	60000	J mol^{-1}
E_j	energy of activation of J_{max}	30000	J mol^{-1}
E_{Γ^*}	energy of activation of the CO_2 compensation point	37830	J mol^{-1}
δ_{S_v}	V_{cmax} entropy factor	650	J mol^{-1} K^{-1}
δ_{S_j}	J_{max} entropy factor	650	J mol^{-1} K^{-1}
H_{δ_v}	V_{cmax} rate of decrease above the optimum temperature	200000	J mol^{-1}
H_{δ_j}	J_{max} rate of decrease above the optimum temperature	200000	J mol^{-1}

Table S6 Predicted ranges of k_{max} at the 10 sites compared with species-specific measured values of k_{max}

Site name	Climate Predicted k_{max} (mmol m^{-2} s^{-1} MPa^{-1})			Measured k_{max} (mmol m^{-2} s^{-1} MPa^{-1})		
	segment	**min.**	**max.**	**min.**	**max.**	**Reference study**
Hyytiälä	branch	1.1	5.8*	1.6[b]	9.5[b]	Martínez-Vilalta & Piñol (2002)
Sorø	branch	4.1	13.4*	2.9[c]	16.7[c]	Lemoine *et al.* (2002)
Loobos	branch	1.9	8.6*	1.6[b]	9.5[b]	Martínez-Vilalta & Piñol (2002)
Hesse Forest-Sarrebourg	branch	11.8*	43.0	2.9[c]	16.7[c]	Lemoine *et al.* (2002)
Parco Ticino Forest	leaf	16.6	57.7*	12	39	Aasamaa *et al.* (2005)
Puéchabon	branch	2.0	8.0*	7.8[a]	51.9[a]	Limousin *et al.* (2010)
Roccarespampani1	branch	12.3*	43.0	15.4[a,c]		Higgs & Wood (1995)
Roccarespampani2	branch	10.3*	36.4	13.8[a,c]		
El Saler1	branch	1.7*	3.8	3.7[a]	31.2[a]	David-Schwartz *et al.* (2016)
Espirra	branch	2.9*	7.7	4.1[a]	73.1[a]	Pita *et al.* (2003)

All the values of k_{max} are expressed per unit area (i.e. our soil-plant k_{max} predictions were first multiplied by the sites' weighted composite LAI to convert from per unit leaf area to per unit area)

* Indicates the value which corresponds to the best performing climate scenario (i.e. the minimum values are given by the minimum between $k_{max,opt}$ and $k_{max,low}$ from the Average Climate scenario whilst the maximum values are given by the maximum between $k_{max,opt}$ and $k_{max,high}$ from the Extreme Climate scenario)

[a] These values were originally expressed in kg m^{-1} s^{-1} MPa^{-1}, which we converted to mmol m^{-2} s^{-1} MPa^{-1} using the molar mass of water and the ratio of hydraulic segment area to hydraulic segment length as reported in the reference study

[b] These values were originally expressed in m^2 s^{-1} MPa^{-1}, which we first converted to kg m^{-1} s^{-1} MPa^{-1} using the hydraulic segment's length and the ratio of water mass per volume water, before further converting to mmol m^{-2} s^{-1} MPa^{-1} using the molar mass of water and the ratio of hydraulic segment area to hydraulic segment length as reported in the reference study

[c] These values were converted from per unit area leaf to per unit area by multiplying by the sites' weighted composite LAI

Supporting Information Methods

Methods S1 Biochemical photosynthesis model

Net photosynthetic demand from the plant (A_n; µmol m^{-2} s^{-1}) is represented following Farquhar *et al.* (1980), including the Rubisco limited photosynthetic rate (A_c; µmol m^{-2} s^{-1}) and the electron transport limited rate (A_j; µmol m^{-2} s^{-1}), with a smoothed hyperbolic transition between the two limitations (Kirschbaum & Farquhar, 1984). The third possible limitation by triose-phosphate at high CO_2 is excluded, as it is rarely reached under present conditions.

$$A_n = \frac{A_c + A_j - \sqrt{(A_c + A_j)^2 - 4\,h\,A_c\,A_j}}{2\,h} - R_d \qquad (1)$$

where h is a unitless transition curvature factor and R_d (µmol m^{-2} s^{-1}) is the dark respiration (see Eqn S5).

The expressions of the Rubisco limited rate, A_c (µmol m^{-2} s^{-1}), and of the electron transport limited rate were obtained from De Pury & Farquhar (1997) :

$$A_c = \frac{V_{cmax}(C_i - \Gamma^*)}{C_i + K_m} \qquad (2)$$

where V_{cmax} (µmol m^{-2} s^{-1}) is the photosynthetic Rubisco capacity scaled up per unit canopy area (i.e. shaded or sunlit; Wang & Leuning, 1998), C_i (Pa) is the intercellular CO_2 partial pressure, Γ^* (Pa) is the CO_2 compensation point of photosynthesis. K_m (Pa) is the effective Michaelis-Menten constant:

$$K_m = K_c \left(1 + \frac{O_a}{K_o}\right) \qquad (3)$$

where K_c (Pa) is the Michaelis-Menten constant of Rubisco for CO_2, K_o (Pa) the Michaelis-Menten constant of Rubisco for O_2, and O_a (Pa) is the atmospheric oxygen partial pressure.

The second limitation, A_j (µmol m^{-2} s^{-1}), is expressed as:

$$A_j = \frac{J\,(C_i - \Gamma^*)}{4\,(C_i + 2\Gamma^*)} \qquad (4)$$

where J (µmol m^{-2} s^{-1}) is the irradiance dependence of electron transport, such as:

$$J = \frac{\alpha Q + J_{max} - \sqrt{(\alpha Q + J_{max})^2 - 4c\alpha Q J_{max}}}{2c} \qquad (5)$$

where α (mol photon mol^{-1} electron) is the effective quantum yield of electron transport depending on leaf emissivity, Q (µmol m^{-2} s^{-1}) is the photosynthetic photon flux density, J_{max} (µmol m^{-2} s^{-1}) is the maximum rate of electron transport scaled up per unit canopy area, and c defines the unitless curvature of the leaf response of electron transport to irradiance.

The temperature dependency of Γ^*, K_c, and K_o is modelled using an Arrhenius function relative to 25 °C, as expressed in De Pury & Farquhar (1997).
The temperature dependency of V_{cmax} and J_{max} is modelled using a peaked Arrhenius function relative to 25 °C, to account for limitations at high temperature, as in Medlyn *et al.* (2002). To account for low temperatures effects (i.e. below 10°C), we simply apply a linear ramp. We also assume co-variation of $V_{cmax,25}$ and $J_{max,25}$, with $J_{max,25}$: $V_{cmax,25} = 1.67$ (Medlyn *et al.*, 2002).

The leaf dark respiration is expressed following Tjoelker *et al.* (2001) at the leaf level:

$$R_d = R_{d,25}(3.22 - 0.046 - T_{leaf})^{\left(\frac{T_{leaf}-25}{10}\right)} \quad (6)$$

where $R_{d,25}$ (µmol m^{-2} s^{-1}) is the reference leaf respiration at 25°C and T_{leaf} (°C) is the leaf temperature for either the sunlit or the shaded fraction of the canopy. R_d is subsequently scaled up per unit canopy area following Wang & Leuning (1998).

Methods S2 Energy balance model

Leaf temperature (T_{leaf}) plays a key regulating role in the above-described photosynthesis model. For example, not only is it used to calculate R_d, but it is also used to yield a suite of canopy-scaled kinetic variables (e.g. V_{cmax} – the temperature dependent maximum carboxylation rate) from their reference at a specific leaf temperature (e.g. $V_{cmax,25}$ – which is at $T_{leaf} = 25$ °C).

Here, T_{leaf} is expressed from rearranging the Penman-Monteith energy balance function for leaves, following equation 14.6 of Campbell & Norman (1998):

$$T_{leaf} = T_{air} + \frac{H}{C_p g_H + \lambda s g_x} \quad (7)$$

where T_{air} (°C) is air temperature, H (W m^{-2}) is the canopy leaf-specific sensible heat flux, C_p (J mol^{-1} °C^{-1}) is the specific heat capacity of dry air at constant pressure, g_H (mol m^{-2} s^{-1}) is total leaf conductance to heat, λ is latent heat of vaporisation (J mol^{-1}), s is the slope of the saturation vapour pressure deficit of water (kPa °C^{-1}), and g_x (mol m^{-2} s^{-1}) either stands for g_b, the leaf boundary conductance to water vapour in the case of the Profit$_{max}$ model, or for g_w, the total leaf conductance to water vapour in the case of the Control model.

For the Profit$_{max}$ model, we note that using g_b instead of g_w in Eqn S7 might have an effect on leaf temperature upon stomatal closure, however stomatal effects ought to be reflected in the vulnerability curve used to determine the transpiration (E; cf. Eqn 4).

Methods S3 Shape of the vulnerability curves

The sensitivity (b, MPa) and shape (c, unitless) parameters used to model the cumulative Weibull distribution (Neufeld *et al.*, 1992) were derived from two values of water potential drop in xylem hydraulic conductivity, such that:

$$b = \frac{P_{x_1}}{(-Log_e(1-x_1/100))^{\frac{1}{c}}} \quad (8)$$

$$c = \frac{Log_e\left(\frac{Log_e(1-x_1/100)}{Log_e(1-x_2/100)}\right)}{Log_e P_{x_1} - Log_e P_{x_2}} \quad (9)$$

where x_1 and x_2 are two percentage values of hydraulic conductivity loss and P_{x_1} and P_{x_2} their associated water potentials (MPa).

Increasing stomatal control, via a decrease in the percentage associated with critical hydraulic conductivity loss (Ψ_{crit}), effectively shortens the transpiration stream on which the Profit$_{max}$ algorithm is applied. As a result, varying Ψ_{crit} is the model's equivalent of rescaling the vulnerability curve, i.e. of changing b. For example, in certain species, complete hydraulic failure leading to death could occur between P_{x_1} and P_{x_2}, in which case setting a specific value of Ψ_{crit} is useful.

Methods S4 Coupling carbon and water

The unified stomatal optimisation model (Medlyn *et al*., 2011) relates stomatal conductance (g_s, mol m^{-2} s^{-1}) to the net rate of carbon assimilation (A_n) using two empirically fitted parameters, g_0 (mol m^{-2} s^{-1}) and g_1 ($kPa^{0.5}$). When embedding the Medlyn *et al.* (2011) model in a LSM, it can be reworked to account for soil moisture stress (Wang *et al.*, 2011):

$$g_s \approx g_0 + 1.57\left(1 + \frac{g_1\beta}{\sqrt{D_{leaf}}}\right)\frac{A_n}{C_s} \qquad (10)$$

where β is the empirical soil-moisture stress factor, D_{leaf} (kPa) is leaf-to-air vapour pressure deficit, C_s is leaf surface CO_2 concentration, and the factor 1.57 converts from conductance to CO_2 to conductance to water vapour. We assume g_0 to be negligible ($1e^{-9}$ mol m^{-2} s^{-1}), an assumption shared with CABLE.

For the Control model, the energy balance is attained in the standard way, by iterating on C_s (starting from C_a), and then on g_s, which sets the new T_{leaf} and D_{leaf}, until the iterations of the shaded or sunlit leaf temperature converge.

For the $Profit_{max}$ model, transpiration (E) is expressed for the shaded and sunlit leaves, following Eqn 4 of the Main text. Since C_i is solved for by equalising Eqns 6 and S1, there is no need for iteration.

For both the Control and the $Profit_{max}$, the expression for T_{leaf} is presented in Methods S2.

Methods S5 Scaling from leaf to canopy

All calculated variables (e.g. canopy conductance values, T_{leaf}) are differentiated between sunlit and shaded leaves. In the $Profit_{max}$ approach, $\Psi_{leaf,opt}$ is also differentiated between sunlit and shaded leaves.

Parameters for the shaded and sunlit leaves are scaled up to the canopy, depending on light scattering, leaf area index, and leaf nitrogen (see Wang & Leuning, 1998). Inside the

biochemical photosynthesis model, V_{cmax}, J_{max}, and $R_{d,25}$ are scaled in this manner, so as to be specific to either the shaded or the sunlit portion of the canopy.

In the case of the $Profit_{max}$ model, the transpiration stream is independent from the Penman-Monteith energy balance function. Therefore, E needs to be scaled up by applying the same scaling factors applied inside the biochemical photosynthesis model, to create shaded and sunlit transpiration streams.

Methods S6 Soil hydrology

Bare soil evaporation is assumed to occur at the equilibrium rate (Monteith & Unsworth, 1990), corrected according to vegetation cover (Ritchie, 1972) and limited by a percentage soil resistance to evaporation (r_{soil}). Soil hydrology is represented by a multi-layer water balance 'tipping bucket' model, where the top layer alone allows soil evaporation. Besides the top layer, with a fixed depth of 2.2 cm, there are five sub-soil layers, for a combined varying depth which varies by site (cf. Table S1).

Transpiration occurs from all the layers, in a top down order (i.e. from the topmost layer which contains water through to the immediately lower layer upon top layer dry-down). The amount of water available for transpiration in each of the five sub-soil layers was derived from the percentages of root water access in CABLE's sub-soil layers (cf. Table S4).

Runoff is not mechanistically represented; instead, a saturation threshold (i.e. θ_{sat} (m^3 m^{-3}), the volumetric soil moisture content at saturation) is set to define the conversion of throughfall to runoff. Upon saturation of the top soil layer, residual precipitation infiltrates the immediate lower layer and is subject to a drainage rate, following Darcy's law and depending on soil hydraulic conductivity (see the methods used in CABLE; Kowalczyk *et al.*, 2006). Vertical movement of soil moisture is simulated by transferring the residual infiltrated water to the immediate lower layer, upon saturation of each layer. Any remaining soil water, upon saturation of the lowest layer, is lost from the system as drainage.

Finally, the overall weighted volumetric soil moisture is calculated and used to characterise the

total amount of water available to the vegetation at any point, with no regard for root distribution. The corresponding soil water potential is given by the Clapp and Hornberger equation (Clapp & Hornberger, 1978):

$$\Psi_s = \Psi_{aep}\left(\frac{\theta}{\theta_{sat}}\right)^{b_{CH}} \qquad (11)$$

where Ψ_s (MPa) is the root zone soil water potential, Ψ_{aep} (MPa) is the air entry point water potential, θ ($m^3\ m^{-3}$) is volumetric soil moisture content, θ_{sat} ($m^3\ m^{-3}$) is the volumetric soil moisture content at saturation, and b_{CH} (unitless) is the Clapp-Hornberger pore size distribution index which approximates the slope of the soil-water retention curve.

Methods S7 Prescribed LAI

a) Site-specific LAI phenologies used to run the model

Each site's LAI was averaged with its immediate surrounding grid cells (i.e. in a 1.5 km radius around the tower) for all the data points in the MODIS release time period until 22-09-2018, only keeping the highest ('good') quality data produced by the main radiative transfer algorithm. Yearly climatologies were then created, by interpolating the three times extrapolated MODIS LAI data, before splining it to account for edges and cloud artefacts.

b) Average growing season weighted LAI used to calculate k_{max}

To calculate values of k_{max} representative of each site, we needed to take into account the LAI for which the stand's photosynthetic productivity would be maximised (i.e. not constrained by soil moisture stress). We opted to calculate the average 'composite' LAI, which we defined as the average of the multi-year sunlit and shaded weighted LAI over the growing season.

The site-specific LAI phenologies were separated into sunlit and shaded LAI fractions for every day-time hour of the growing season (i.e. April – November) between 1972 – 2002. We separated the LAI using the radiation at the top of the atmosphere (Spitters *et al.*, 1986), reduced by the CRU TS v4.03 dataset's monthly daily average cloud cover (Harris *et al.*, 2014)

following the empirical correction formula derived by Nikolov & Zeller (1992). Secondly, we weighted the sunlit and shaded LAI into a composite LAI for every day of the growing season. Finally, we selected the average value of this composite LAI, and used it for internal scaling from leaf to canopy (cf. Methods S5) when calculating the site's k_{max}.

Methods S8 Parameter calibrations

a) Effective rooting depths (Z_{total})

We calibrated Z_{total} to maximise the Control model's performance in simulating ET compared with the observations of ET between April – July for all the simulated years, using the same quantile ranking system than that used to select k_{max} in the Main text, Section 6a of the Methods. We prevented calibrating for relatively large soil evaporation biases (i) by rescaling the mean square error metrics (i.e. the NMSE), changing the normalisation factor from $1/(\overline{obs} \times \overline{sim})$ to $\overline{obs}/\overline{sim}$; (ii) by introducing an additional criterion in the selection process, whereby we excluded any value of Z_{total} for which the total contribution of the transpiration to ET fell below 70% (Stoy *et al.*, 2019). To ensure that the calibration was performed using sensible soil moisture states at the beginning of each of the runs (i.e. for 2002, 2003, 2005, and 2006), we also reran all the spin-ups for each of the possible values of Z_{total}. Finally, the possible range of calibrated Z_{total} was restricted between the half of each site's effective rooting depth as given by CABLE (c. 0.25 m) and increased up to 1.5 m, by increments of 0.05 m.
The obtained "best" calibrated Z_{total} are similar to those shown by Yang *et al.* (2016) over Europe.

b) Calibrating g_1

To calibrate g_1 in the Control model, we first generated a sequence of possible values for g_1. 12 values were evenly selected between 25% – 95% of the reference site-specific g_1 values presented in Table S2 and a further 12 values were evenly distributed between 105% – 400% of the reference g_1. The reference g_1 itself was added to the sequence, which in total led to 25 values being used as parameter inputs to run each of the drought and non-drought years. The

best calibrated g_1 value was selected following the procedure detailed in Section 6a of the Materials and Methods.

c) Calibrating the soil moisture stress factor (β)

To calibrate β, we transformed the relationship to soil moisture content in two ways: 1) we applied a power factor to the expression of β; 2) we added correction terms around the point of stomatal closure (i.e. the wilting point defined at a threshold of -1.5MPa and based on soil texture parameters) and the point of maximal stomatal openness (i.e. the soil field capacity). The new expression of β was as follows:

$$\beta = \left(\frac{\theta - (\theta_{wp}+b)}{(\theta_{fc}+c)-(\theta_{wp}+b)}\right)^{a} \qquad (12)$$

where θ ($m^3\ m^{-3}$) is volumetric soil moisture and θ_{wp} ($m^3\ m^{-3}$) and θ_{fc} ($m^3\ m^{-3}$) are the volumetric soil moisture contents at wilting point and field capacity, respectively. a is a unitless power factor, b ($m^3\ m^{-3}$) and c ($m^3\ m^{-3}$) are correction terms applied on the soil moisture contents at wilting point and field capacity, respectively.

We then generated sequences of possible values for a, b, and c. The sequence for a consisted in 10 linearly sampled values between 0.1 and 1 and of a further 10 linearly sampled values between 1 and 10. The sequence for b was -0.1, -0.05, 0, and 0.05. The sequence for c was -0.05, 0, 0.05 and 0.1. The final β factors which were used to run each of the drought and non-drought years were generated by combining the sequences of a, b, and c, which led to 300 unique combinations. The best calibrated β was selected following the procedure detailed in Section 6a of the Materials and Methods.

New Phytologist

Supporting Information Notes

Notes S1 Comparison of the Control with CABLE

The TractLSM was meant to mimic a standard LSM is such a way that would make our findings general and not necessarily specific to a single LSM. Here, because we compare it with CABLE, we first discuss the important similarities and differences between the TractLSM and CABLE.

In its standard configuration (i.e. the Control model), the TractLSM's routines used to estimate E and A_n are similar to the default CABLE. We use the same biochemical photosynthesis model (cf. Methods S1), parameterised in the same way, with the exception of the leaf dark respiration which is calculated according to Tjoelker *et al.* (2001) whilst CABLE assumes it to be 0.015 * $V_{c,max25}$. Our ensuing leaf-level energy balance calculations are the same as in CABLE (see Methods S4) and so is our scaling from leaf-to-canopy using a two-leaf approximation and a full canopy radiation budget (cf. Methods S5). However, it must be noted that CABLE uses a single averaged T_{leaf} over the shaded and sunlit fractions of the canopy between two iterations on the leaf-level energy balance, which likely introduces uncertainties in the GPP and ET estimates, whereas the TractLSM model keeps the shaded and sunlit T_{leaf} separated. During iterations at each timestep, most LSMs perform a series of stability corrections following the Monin-Obukhov stability theory. In our simplified model we did not perform these stability corrections because we found them to be negligible in CABLE during the growing season (i.e. at all of our sites, they amount to < 0.5°C corrections on air temperature on average over a year and are only significant outside of the growing season when LAI is near zero).

The TractLSM's simulation of soil evaporation and hydrology, however, diverges from CABLE's. Firstly, there is no explicit representation of runoff in the TractLSM, as it is set by the excess rainfall which cannot infiltrate the soil when near surface volumetric soil moisture content has reached the point of saturation. Secondly, the TractLSM simulates a unique soil temperature across all 6 soil layers, using the previous day's average meteorological temperature. So, soil temperature does not vary through the day as in CABLE.

Despite these simplifications, the Control model simulated GPP and ET fluxes broadly comparable to CABLE, at all sites, both during drought (cf. Fig. S2 and S3) and outside of drought periods (not shown). The Control model also seemingly performed better than CABLE at e.g. Hesse or Parco Ticino. One possible reason why that might be is that, despite its relative lack of sophistication, the Control model uses effective rooting depth (i.e. the actual amount of water which is extractable for the plant) and that we have adjusted the effective rooting depth on a per-site basis. In spite of using adjusted effective rooting depths, a method supported by the existing literature on tipping bucket models (Martens et al., 2017; Stocker et al., 2018), most sites show soil moisture profiles comparable to CABLE, with regards to their dynamics between April - November (cf. Fig. S4 and S5). However, the Control model's total depth (i.e. effective rooting depth) is always shallower than CABLE's total rooting depth, but equal or deeper than CABLE's effective rooting depth, and so changes in soil moisture are steeper in the Control than in CABLE (e.g. Loobos in Fig. S4).

Notes S2 Why did we not calibrate the Control model?

An argument can be made in favour of calibrating existing processes in state-of-the-art LSMs, rather than changing the structure of these complex models. In the case of stomatal control, calibration pertains to two different processes: the water use efficiency term (here, this is g_1 from the Medlyn *et al.* (2011) model) and the soil moisture stress factor (β). We wanted to establish whether calibration led to physically meaningful model improvement. To achieve this, we ran 25 different calibrations of g_1 (cf. Methods S8b) and 300 calibrations of the β function (cf. Methods S8c) for all the years and sites examined in this study; this led to >10,000 model runs.

Calibrating g_1 led to improved or equivalent model performance in simulating ET outside of drought (i.e. in 2002 and 2005) at all sites, compared with the reference Control model. However, this was not the case at all sites during drought (i.e. 2003 and 2006), with for example a marked decrease at Sorø for every statistical metric of performance. Overall compared with the reference Control model, ET deviations (i.e NMSE) were reduced by c. 37%. Accuracy

increased (i.e. the MAE decreased) by c. 17% and the error in variability (i.e. SD metric) decreased by c. 33%. Finally, the ability to capture the tails of the distribution increased by 9% for the p_5 metric and by 46% for the p_{95} metric. Improvements in simulating the lower tail of the ET distribution aside, the above listed improvements are all smaller than those achieved by the best calibration from the Profit_{max} model (cf. Section 1 of the Results in the Main text). Although calibrating g_1 in the Control model noticeably improved the simulation of ET at Hyytiäla (cf. Fig. S6b, d, f, h), the calibrated Control model did not outperform the calibrated Profit_{max} model for any of the five statistical metrics of performance at this site (e.g. the ET NMSE is 0.065 in the calibrated Profit_{max} model across years versus 0.15 in the calibrated Control model). Importantly, the best calibrated values of g_1 for the Control model ranged between 1.04 – 7.06 $\text{kPa}^{0.5}$ and markedly departed from the measured g_1 data at Hyytiäla (calibrated value of 4.82 $\text{kPa}^{0.5}$ versus measured value of 1.29 $\text{kPa}^{0.5}$) and Puéchabon (calibrated value of 4.16 $\text{kPa}^{0.5}$ versus measured value of 1.56 $\text{kPa}^{0.5}$). These results imply that the Control model is able to capture improved performance for the wrong mechanistic reasons.

Calibrating β led to marginal improvements in the simulation of ET across sites in the non-drought years (ET deviations were reduced by c. 25%), but not during drought (ET deviations increased by c. 2%). Even though calibrating β ought to help capture plants' sensitivity to water stress, it is unclear from Figure S6q what such a calibration would physiologically mean. Looking at the calibrated β at Hyytiälä, stomata go from fully open to fully closed in under 0.02 $\text{m}^3\ \text{m}^{-3}$, therefore displaying very high stomatal control, at odds with the measured hydraulic traits of *P. sylvestris* (cf. Table S2). These results corroborate the findings of (Verhoef & Egea, 2014) who showed that the performance of altered β remained poor compared with that of plant water stress relationships found from hydraulic models.

Notes S3 Comparison of the predicted values of k_{max} to the literature

To assess whether the values that we calculated for k_{max} based on the sites' climate are sensible, we compared their ranges to measured values of k_{max} reported in the literature. k_{max} is often measured for a specific hydraulic segment, whereas our predicted values are valid

over the full soil-plant continuum. This means we cannot directly compare our predictions to literature values without making a scaling assumption to segment values between components of the soil-plant continuum.

Here we assumed that: 10% of the resistance from the soil-plant continuum is in a plant's branches (Yang & Tyree, 1994), and 30% of the whole resistance is in its leaves (Sack & Holbrook, 2006). We acknowledge that this is a simplistic assumption that does not capture inter-specific and site differences in hydraulic segmentation. As a result, our comparisons, presented in Table S6, are merely indicative of agreement with our estimated values of k_{max}.

Table S6 shows that our estimates of k_{max} from the climate scenarios (with ranges that envelope all of our calibrated estimates of k_{max}) to match not only the magnitude of the measured k_{max}, but the best estimates from the best climate scenarios to also fall within the range of measured k_{max} at seven out of 10 sites (they do not at Parco Ticino, El Saler1, and Espirra).

References

Aasamaa K, Niinemets U, Sober A. **2005**. Leaf hydraulic conductance in relation to anatomical and functional traits during Populus tremula leaf ontogeny. *Tree Physiology* **25**: 1409–1418.

Berge HFM ten. **1990**. *Heat and water transfer in bare topsoil and lower atmosphere*. Wageningen: Pudoc.

Campbell GS, Norman JM. **1998**. *An Introduction to Environmental Biophysics*. New York, NY: Springer New York.

Clapp RB, Hornberger GM. **1978**. Empirical equations for some soil hydraulic properties. *Water Resources Research* **14**: 601–604.

David-Schwartz R, Paudel I, Mizrachi M, Delzon S, Cochard H, Lukyanov V, Badel E, Capdeville G, Shklar G, Cohen S. **2016**. Indirect Evidence for Genetic Differentiation in Vulnerability to Embolism in Pinus halepensis. *Frontiers in Plant Science* **7**. doi : 10.3389/fpls.2016.00768

De Kauwe MG, Kala J, Lin Y-S, Pitman AJ, Medlyn BE, Duursma RA, Abramowitz G, Wang Y-P, Miralles DG. **2015**. A test of an optimal stomatal conductance scheme within the CABLE land surface model. *Geoscientific Model Development* **8**: 431–452.

De Pury DGG, Farquhar GD. **1997**. Simple scaling of photosynthesis from leaves to canopies without the errors of big-leaf models. *Plant, Cell and Environment* **20**: 537–557.

Duursma RA, Kolari P, Peramaki M, Nikinmaa E, Hari P, Delzon S, Loustau D, Ilvesniemi H, Pumpanen J, Makela A. **2008**. Predicting the decline in daily maximum transpiration rate of two pine stands during drought based on constant minimum leaf water potential and plant hydraulic conductance. *Tree Physiology* **28**: 265–276.

Farquhar GD, Caemmerer S von, Berry JA. **1980**. A biochemical model of photosynthetic CO2 assimilation in leaves of C3 species. *Planta* **149**: 78–90.

Harris I, Jones PD, Osborn TJ, Lister DH. **2014**. Updated high-resolution grids of monthly climatic observations - the CRU TS3.10 Dataset. *International Journal of Climatology* **34**: 623–642.

Higgs K, Wood V. **1995**. Drought susceptibility and xylem dysfunction in seedlings of 4 European oak species. *Annales des Sciences Forestières* **52**: 507–513.

Kattge J, Knorr W, Raddatz T, Wirth C. **2009**. Quantifying photosynthetic capacity and its relationship to leaf nitrogen content for global-scale terrestrial biosphere models. *Global Change Biology* **15**: 976–991.

Kirschbaum M, Farquhar G. **1984**. Temperature Dependence of Whole-Leaf Photosynthesis in Eucalyptus pauciflora Sieb. Ex Spreng. *Functional Plant Biology* **11**: 519.

Kowalczyk EA, CSIRO Marine and Atmospheric Research. **2006**. *The CSIRO Atmosphere Biosphere Land Exchange (CABLE) model for use in climate models and as an offline model*. Aspendale, Vic.: CSIRO Marine and Atmospheric Research.

Lemoine D, Cochard H, Granier A. **2002**. Within crown variation in hydraulic architecture in beech (*Fagus sylvatica* L): evidence for a stomatal control of xylem embolism. *Annals of Forest Science* **59**: 19–27.

Limousin J-M, Longepierre D, Huc R, Rambal S. **2010**. Change in hydraulic traits of Mediterranean Quercus ilex subjected to long-term throughfall exclusion. *Tree Physiology* **30**: 1026–1036.

Lin Y-S, Medlyn BE, Duursma RA, Prentice IC, Wang H, Baig S, Eamus D, de Dios VR, Mitchell P, Ellsworth DS, *et al.* 2015. Optimal stomatal behaviour around the world. *Nature Climate Change* **5**: 459–464.

Lucani CJ, Brodribb TJ, Jordan G, Mitchell PJ. **2019**. Intraspecific variation in drought susceptibility in Eucalyptus globulus is linked to differences in leaf vulnerability. *Functional Plant Biology* **46**: 286.

Martens B, Miralles DG, Lievens H, van der Schalie R, de Jeu RAM, Fernández-Prieto D, Beck HE, Dorigo WA, Verhoest NEC. **2017**. GLEAM v3: satellite-based land evaporation and root-zone soil moisture. *Geoscientific Model Development* **10**: 1903–1925.

Martin-StPaul NK. **2012**. Functional adjustments of holm oak (Quercus ilex L.) facing increasing drought at different temporal scales: Impacts for process based modeling. Ph.D. thesis (364 p.), Université de Montpellier II, France.

Martin-StPaul N, Delzon S, Cochard H. **2017**. Sureau Database : A Database Of Hydraulic And Stomatal Traits For Modelling Drought Resistance In Plants. doi : 10.5281/zenodo.854700

Martínez-Vilalta J, Piñol J. **2002**. Drought-induced mortality and hydraulic architecture in pine populations of the NE Iberian Peninsula. *Forest Ecology and Management* **161**: 247–256.

Medlyn BE, Dreyer E, Ellsworth D, Forstreuter M, Harley PC, Kirschbaum MUF, Le Roux X, Montpied P, Strassemeyer J, Walcroft A, *et al.* 2002. Temperature response of parameters of a biochemically based model of photosynthesis. II. A review of experimental data. *Plant, Cell and Environment* **25**: 1167–1179.

Medlyn BE, Duursma RA, Eamus D, Ellsworth DS, Prentice IC, Barton CVM, Crous KY, De Angelis P, Freeman M, Wingate L. **2011**. Reconciling the optimal and empirical approaches to modelling stomatal conductance. *Global Change Biology* **17**: 2134–2144.

Monteith JL, Unsworth MH. **1990**. *Principles of environmental physics*. London ; New York : New York: E. Arnold ; Distributed in the USA by Routledge, Chapman and Hall.

Neufeld HS, Grantz DA, Meinzer FC, Goldstein G, Crisosto GM, Crisosto C. **1992**. Genotypic Variability in Vulnerability of Leaf Xylem to Cavitation in Water-Stressed and Well-Irrigated Sugarcane. *Plant Physiology* **100**: 1020–1028.

Nikolov NT, Zeller KF. **1992**. A solar radiation algorithm for ecosystem dynamic models. *Ecological Modelling* **61**: 149–168.

Pita P, Gascó A, Pardos JA. **2003**. Xylem cavitation, leaf growth and leaf water potential in Eucalyptusglobulus clones under well-watered and drought conditions. *Functional Plant Biology* **30**: 891-899.

Ritchie JT. **1972**. Model for predicting evaporation from a row crop with incomplete cover. *Water Resources Research* **8**: 1204–1213.

Sack L, Holbrook NM. **2006**. Leaf Hydraulics. *Annual Review of Plant Biology* **57**: 361–381.

Spitters CJT, Toussaint HAJM, Goudriaan J. **1986**. Separating the diffuse and direct component of global radiation and its implications for modeling canopy photosynthesis Part I. Components of incoming radiation. *Agricultural and Forest Meteorology* **38**: 217–229.

Stocker BD, Zscheischler J, Keenan TF, Prentice IC, Peñuelas J, Seneviratne SI. **2018**. Quantifying soil moisture impacts on light use efficiency across biomes. *New Phytologist* **218**: 1430–1449.

Stoy PC, El-Madany TS, Fisher JB, Gentine P, Gerken T, Good SP, Klosterhalfen A, Liu S, Miralles DG, Perez-Priego O, *et al.* 2019. Reviews and syntheses: Turning the challenges of partitioning ecosystem evaporation and transpiration into opportunities. *Biogeosciences* **16**: 3747–3775.

Tjoelker MG, Oleksyn J, Reich PB. **2001**. Modelling respiration of vegetation: evidence for a general temperature-dependent Q10. *Global Change Biology* **7**: 223–230.

Valentini R (Ed.). **2003**. *Fluxes of Carbon, Water and Energy of European Forests*. Berlin, Heidelberg: Springer Berlin Heidelberg.

Van den Hoof C, Vidale PL, Verhoef A, Vincke C. **2013**. Improved evaporative flux partitioning and carbon flux in the land surface model JULES: Impact on the simulation of land surface processes in temperate Europe. *Agricultural and Forest Meteorology* **181**: 108–124.

Verhoef A, Egea G. **2014**. Modeling plant transpiration under limited soil water: Comparison of different plant and soil hydraulic parameterizations and preliminary implications for their use in land surface models. *Agricultural and Forest Meteorology* **191**: 22–32.

Wang Y-P, Kowalczyk E, Leuning R, Abramowitz G, Raupach MR, Pak B, van Gorsel E, Luhar A. **2011**. Diagnosing errors in a land surface model (CABLE) in the time and frequency domains. *Journal of Geophysical Research* **116**. doi : 10.1029/2010JG001385

Wang Y-P, Leuning R. **1998**. A two-leaf model for canopy conductance, photosynthesis and partitioning of available energy I: *Agricultural and Forest Meteorology* **91**: 89–111.

Yang Y, Donohue RJ, McVicar TR. **2016**. Global estimation of effective plant rooting depth: Implications for hydrological modeling. *Water Resources Research* **52**: 8260–8276.

Yang S, Tyree MT. **1994**. Hydraulic architecture of *Acer saccharum* and *A. rubrum* : comparison of branches to whole trees and the contribution of leaves to hydraulic resistance. *Journal of Experimental Botany* **45**: 179–186.

Zobler L. **1999**. GLOBAL SOIL TYPES, 1-DEGREE GRID (ZOBLER).